VOLUME 112, NUMBER 2
JANUARY 17, 1990

JOURNAL
OF THE
AMERICAN
CHEMICAL
SOCIETY

Excited-State Racemization Kinetics and Chiroptical Activity of a Labile Metal Complex in Aqueous Solution. Time-Resolved Circularly Polarized Luminescence Study of $Eu(dpa)_3^{3-}$ in H_2O and D_2O

David H. Metcalf,*,† Seth W. Snyder,‡ J. N. Demas,† and F. S. Richardson*,†

Contribution from the Chemistry Department and Biophysics Program, University of Virginia, Charlottesville, Virginia 22901. *Received July 24, 1989*

Abstract: Time-resolved circularly polarized luminescence (TR-CPL) measurements are used to characterize the excited-state chiroptical activity and racemization kinetics of $Eu(dpa)_3^{3-}$ (dpa ≡ dipicolinate) in H_2O and D_2O solutions at temperatures between 293 and 353 K. Racemic $Eu(dpa)_3^{3-}$ is excited with circularly polarized light to create an enantiomeric excess of one optical (configurational) isomer in an excited electronic state, and then comparisons between time-resolved *total* luminescence and *circularly polarized* luminescence spectra are used to monitor the time dependence of the enantiomeric excess. Decay of the enantiomeric excess is related to interconversion of optical isomers (i.e., racemization) within the excited-state population of complexes, and rate constants are determined for the excited-state racemization of $Eu(dpa)_3^{3-}$ in both H_2O and D_2O over a 60 °C temperature range. Arrhenius parameters and thermodynamic activation parameters are derived from the temperature-dependent rate data, and the results obtained in H_2O and D_2O are compared and discussed. The racemization lifetimes (the reciprocal of the racemization rate constants) determined for 293 K solutions (31.6 and 45.5 ms in H_2O and D_2O, respectively) are long compared to the emission lifetimes (1.60 and 3.19 ms, respectively). The racemization process is interpreted in terms of an *intramolecular* mechanism without any (complete or partial) ligand dissociation. The complex passes through an achiral transition state of either D_{3h} or C_{2v} symmetry during interconversions between the two D_3 enantiomers. Circularly polarized luminescence spectra are presented for the $^7F_{0,1,2} \leftarrow {}^5D_0$ transition regions of europium(III) in $Eu(dpa)_3^{3-}$, and circularly polarized excitation spectra are reported for the $^7F_{0,1} \rightarrow {}^5D_1$ transition regions. The latter are analogous to circular dichroism spectra one would obtain from resolved (nonracemic) samples of $Eu(dpa)_3^{3-}$ in solution. In our experiments, they are the consequence of *chiral photoselection* in the excitation of a racemic mixture with circularly polarized light.

Detailed electronic and stereochemical structure information about lanthanide complexes in solution is elusive. This is particularly true for aqueous solutions wherein most lanthanide complexes exhibit both constitutive and stereochemical lability. Constitutive lability most often reflects ligand-solvent molecule *or* bound ligand-free ligand exchange processes that produce changes in the chemical composition of the inner-coordination sphere, and stereochemical lability reflects configurational and/or conformational isomerization processes within the inner-coordination sphere. These different kinds of structural changes generally occur on different time scales, but it is difficult to characterize them individually. Experimental characterization requires measurements that can be carried out on an appropriate time scale and are diagnostic of the specific structure type of interest. Most experimental studies reported for lanthanide complexes in solution provide time-average or ensemble-average data on properties that can be used, at best, to infer information about equilibrium distributions of (static) structure types. Very little is known about the dynamics of structural changes and structure-type interconversions.

In the study reported here, we investigated a particular kind of *stereochemical* lability that is exhibited by an important (and

* Authors to whom correspondence should be addressed.
† Chemistry Department, University of Virginia.
‡ Biophysics Program, University of Virginia.

0002-7863/90/1512-469$02.50/0

often studied) class of nine-coordinate, tris-terdentate lanthanide(III) complexes in aqueous solution. Examples of complexes in this class are those formed by dipicolinate (dpa) and oxydiacetate (oda) dianions in neutral aqueous solution with Ln^{3+} ions. X-ray structure analyses of crystals containing $Ln(dpa)_3^{3-}$ or $Ln(oda)_3^{3-}$ complexes reveal that these complexes have tris-terdentate chelate structures with trigonal-dihedral (D_3) point-group symmetry.[1-5] The carboxylate oxygen donor atoms form a slightly distorted trigonal prism structure (of D_3 symmetry), and the middle donor atom of each ligand (a pyridyl nitrogen in dpa or an ether oxygen in oda) is located on a normal to one of the rectangular faces of the trigonal prism. The bicyclic chelate ring formed by each ligand is nearly planar, and the ligand backbone of each ring stretches diagonally across one of the rectangular faces of the trigonal prism. Each of the bicyclic chelate rings has a 2-fold symmetry axis that coincides with one of the dihedral axes of the overall (D_3) complex. The tris complex has configurational chirality about its trigonal axis and may form enantiomeric structures (optical isomers). The enantiomeric structures of $Ln(oda)_3^{3-}$ in single-crystal enantiomorphs of trigonal $Na_3[Ln(oda)_3]\cdot 2NaClO_4\cdot 6H_2O$ have been studied extensively by a variety of chiroptical measurement techniques.[6]

There is considerable evidence that the equilibrium structures of $Ln(dpa)_3^{3-}$ and $Ln(oda)_3^{3-}$ complexes in solution are qualitatively identical with those formed in crystals.[7] However, whereas single crystals contain *pure* enantiomers (with either left-handed or right-handed configurational chirality about the trigonal axis of the complex), solution samples contain a *racemic* mixture of enantiomers. *Nonracemic* equilibrium distributions of enantiomers in solution can only be achieved by introducing a chemical or physical (chiral) resolving reagent as a cosolute. Such reagents are commonly referred to as "Pfeiffer reagents", and their effects on distributions of $Ln(dpa)_3^{3-}$ and $Ln(oda)_3^{3-}$ enantiomers in aqueous solution have received considerable attention.[8-11] Steady-state irradiation of a racemic sample with circularly polarized light (in an absorption region of a complex) can also be used to effect partial optical resolution within the ground-state population of complexes, but this resolution is not sustained when the light is turned off. In the absence of chiral reagents, $Ln(dpa)_3^{3-}$ and $Ln(oda)_3^{3-}$ complexes are highly labile with respect to their enantiomeric structures in solution. Characterization of this type of stereochemical lability can provide important information about the structural dynamics of lanthanide chelate systems in solution. In the present study, we focus on just one system, $Eu(dpa)_3^{3-}$, and we use both steady-state and time-resolved chiroptical measurements to characterize the stereochemical lability of this system in aqueous (H_2O and D_2O) solutions.

The $Eu(dpa)_3^{3-}$ system was chosen for study because the optical emission properties of europium are suitable for probing the structural dynamics of interest, and $Ln(dpa)_3^{3-}$ complexes appear not to exhibit constitutive lability on the time scale of interest.[12,13] That is, ligand-solvent exchange and bound ligand-free ligand exchange processes are slow compared to optical enantiomer interconversions, and the complex remains intact on the time scale of these latter (stereochemical) transformations. Our method for studying the dynamics of enantiomer interconversions is based on measurements of racemization rates within a *nonracemic* excited-state population of complexes prepared by a pulse of circularly polarized exciting light.[6,14-16] The circularly polarized excitation creates an excess of one enantiomer over the other (i.e., an enantiomeric excess) in the excited-state population of complexes, and this enantiomeric excess can be monitored by measuring the differential emission of left- and right-circularly polarized light from the sample. In our experiments, both the excitation and emission processes occur via europium 4f-4f electronic transitions, and all intermediate (nonradiative) processes occur within or among states derived from the $4f^6$ electronic configuration of europium. Under these conditions, one may assume that the excited-state structural properties of the complexes will be essentially identical with the ground-state structural properties, since $4f \rightarrow 4f$ excitations (or deexcitations) in lanthanide complexes have little influence on coordination geometry (and chemistry).

Time-resolved, *unpolarized* emission measurements have been used previously by Horrocks and co-workers to determine kinetic parameters for ligand–ligand exchange processes occurring in several kinds of europium(III) coordination systems in aqueous solution.[13] The equilibrium dynamics of chemically distinct species in solution were of principal interest, with the differentiation between species being defined by the number or kind of ligands coordinated directly to the europium ion. Differences in the optical excitation and emission properties of Eu(III) in different species were exploited in characterizing the equilibrium distribution of species and determining the rates of species interconversions. Species of a particular type were *selectively* excited (via narrow-line laser excitation of the Eu(III) $^7F_0 \rightarrow {}^5D_0$ electronic transition), and then the luminescence intensity was monitored as a function of time at several wavelengths within the $^7F_2 \leftarrow {}^5D_0$ transition region of Eu(III). The emission wavelengths were selected to be characteristic of different excited-state species: those formed by the initial excitation event *and* those formed by chemical interconversion processes (among species types) during the time interval between excitation and emission. The measurements and kinetic analyses reported by Horrocks and co-workers[13] yielded valuable information about the constitutive lability and equilibrium distribution of structures for several classes of Eu(III) coordination systems in solution.

The stereochemical lability of interest in this study cannot be investigated by methods in which species differentiation is based on excitation or emission wavelength selectivity, excited-state lifetime selectivity, or differences in unpolarized lifetime decay kinetics. Enantiomeric structures of a chiral system will be identical with respect to each of these differentiation criteria. Spectroscopic differentiation between enantiomers requires chiroptical measurements in which the enantiomers are distinguished by their differential interactions with (or emission of) left- and right-circularly polarized radiation. As was noted earlier, in the study reported here we used circularly polarized light to preferentially excite one enantiomer population of racemic $Eu(dpa)_3^{3-}$ in solution, and then monitored the chiroptical activity of the nonracemic excited-state population of complexes by measuring the differential emission of left- and right-circularly polarized light over the lifetime of the Eu(III) $^5D_0$ emitting state. Following convention, we refer to this differential emission as *circularly polarized luminescence* (CPL)[17] and define it in terms of the observable quantity, $\Delta I = I_l - I_r$, where I_l and I_r denote, respectively, the left- and right-circularly polarized components of the total luminescence intensity. In addition to measuring ΔI as a function of time, we also (simultaneously) measured the quantity, $I = I_l + I_r$, which we refer to as the *total luminescence* (TL). The *emission dissymmetry factor*, g_{em}, is defined as twice the ratio of $\Delta I:I$, and it is the time dependence of this factor that provides the crucial information about excited-state racemization (i.e., enantiomer interconversion) dynamics. In the absence of racemization during the time interval between excitation and complete

(1) Albertsson, J. *Acta Chem. Scand.* **1972**, *26*, 985-1004.
(2) Albertsson, J. *Acta Chem. Scand.* **1972**, *26*, 1005-1017.
(3) Albertsson, J. *Acta Chem. Scand.* **1972**, *26*, 1023-1044.
(4) Albertsson, J. *Acta Chem. Scand.* **1970**, *24*, 3527-3541.
(5) Albertsson, J.; Elding, I. *Acta Chem. Scand.* **1977**, *A31*, 21-30.
(6) Richardson, F. S. *J. Less Common Metals* **1989**, *149*, 161-177.
(7) Foster, D. R.; Richardson, F. S. *Inorg. Chem.* **1983**, *22*, 3996-4002.
(8) Yan, F.; Brittain, H. G. *Polyhedron* **1982** *1*, 195-199.
(9) Hilmes, G. L.; Coruh, N.; Riehl, J. P. *Inorg. Chem.* **1988**, *27*, 1136-1139.
(10) Coruh, N.; Hilmes, G. L.; Riehl, J. P. *Inorg. Chem.* **1988**, *27*, 3647-3651.
(11) Wu, S.; Hilmes, G. L.; Riehl, J. P. *J. Phys. Chem.* **1989**, *93*, 2307-2310.
(12) Donato, H.; Martin, R. B. *J. Am. Chem. Soc.* **1972**, *94*, 4129-4131.
(13) Horrocks, W. D., Jr.; Arkle, V. K.; Liotta, F. J.; Sudnick, D. R. *J. Am. Chem. Soc.* **1983**, *105*, 3455-3459.
(14) Hilmes, G. L.; Riehl, J. P. *J. Phys. Chem.* **1983**, *87*, 3300-3304.
(15) Hilmes, G. L.; Timper, J. M.; Riehl, J. P. *Inorg. Chem.* **1985**, *24*, 1721-1722.
(16) Hilmes, G. L.; Riehl, J. P. *Inorg. Chem.* **1986**, *25*, 2617-2622.
(17) Riehl, J. P.; Richardson, F. S. *Chem. Rev.* **1986**, *86*, 1-16.

emission decay, ΔI and I will exhibit identical time-dependent behavior, and g_{em} will have a constant value. However, if racemization processes are occurring during this time interval, then ΔI will decay faster than I, and g_{em} will display a time dependence that reflects the rate at which the excited-state enantiomeric excess (prepared by circularly polarized excitation) is being depleted by the racemization processes.

Steady-state chiroptical luminescence measurements have been reported previously for racemic $Ln(dpa)_3^{3-}$ complexes excited by circularly polarized light,[15,16] and the theory of time-resolved circularly polarized luminescence (TR-CPL) from systems undergoing racemization processes has been worked out in some detail by Riehl and co-workers.[14] However, this is the first report of TR-CPL measurements on such a system and the first kinetic analysis of optical isomerization dynamics in a lanthanide complex. Previously, we reported the use of TR-CPL measurements to detect and characterize enantioselective interactions between *racemic* $Tb(dpa)_3^{3-}$ and the *resolved* chiral transition-metal complex $Ru(phen)_3^{2+}$ (phen ≡ 1,10-phenanthroline) in aqueous solution.[18] In that study, the $Tb(dpa)_3^{3-}$ was excited with unpolarized light to produce a racemic excited-state population, and then TR-CPL measurements were used to follow the development of an excited-state enantiomeric excess produced by enantioselective quenching of the excited $Tb(dpa)_3^{3-}$ isomers by the resolved $Ru(phen)_3^{2+}$ complex.

Theory and Measurement Methodology

The general theory underlying the experiments and data analyses reported in this paper have been described previously by Riehl and co-workers.[14] In our discussion here, we shall briefly review the relevant aspects of the general theory and, where necessary, adapt it for application to our study of the $Eu(dpa)_3^{3-}$ system. The spectroscopic properties of principal interest in this study are circular dichroism (CD) and circularly polarized luminescence (CPL) associated with 4f–4f electronic transitions in the Eu(III) ion. The CD and CPL observables may be defined as follows: $\Delta A = A_l(\lambda) - A_r(\lambda)$ for CD (measured at wavelength λ), where A_l and A_r denote absorbances for left- and right-circularly polarized light, respectively, and $\Delta I = I_l(\lambda') - I_r(\lambda')$ for CPL (measured at wavelength λ'), where I_l and I_r denote intensities for the left- and right-circularly polarized components of sample luminescence. Also of interest in our experiments are the quantities: $A(\lambda) = [A_l(\lambda) + A_r(\lambda)]/2$, which corresponds to sample absorbance for *unpolarized* light at wavelength λ, and $I(\lambda') = I_l(\lambda') + I_r(\lambda')$, which is proportional to *total(unpolarized)* luminescence intensity at wavelength λ'.

In chiroptical spectroscopy, it is frequently useful to analyze results in terms of *dissymmetry factors* rather than circularly polarized intensity differentials. These factors are unitless and are defined as follows:

$$g_{abs}(\lambda) = \frac{\Delta A(\lambda)}{A(\lambda)} = \frac{\Delta\epsilon(\lambda)}{\epsilon(\lambda)} \tag{1}$$

for CD/absorption measurements (at wavelength λ) and

$$g_{em}(\lambda') = \frac{2\Delta I(\lambda')}{I(\lambda')} \tag{2}$$

for CPL/emission measurements (at wavelength λ'). In these expressions, the ΔA, A, ΔI, and I quantities are defined according to the expressions given in the preceding paragraph: $\Delta\epsilon = \epsilon_l - \epsilon_r$ (the difference in molar absorptivities of left- and right-circularly polarized light) and $\epsilon = (\epsilon_l + \epsilon_r)/2$. These expressions assume Beer–Lambert law behavior in sample absorption and one-photon radiative processes in both absorption and excitation/emission. Neither g_{abs} nor g_{em} depends on sample concentration, and each can be determined from *relative* (as opposed to *absolute*) spectroscopic intensity measurements. Opposite enantiomers of a chiral system will exhibit dissymmetry factors that are equal in magnitude but opposite in sign at any particular absorption or emission wavelength of the system.

Now consider a chiral system that has just one pair of optical isomers (or enantiomers). We label these isomers as Λ (the enantiomer with *left-handed* chirality) and Δ (the enantiomer with *right-handed* chirality). For samples containing a mixture of enantiomers, it is often convenient to characterize the *relative* enantiomer composition of the mixture in terms of *enantiomeric excess*, which we define here as

$$\eta = \frac{[\Lambda] - [\Delta]}{[\Lambda] + [\Delta]} \tag{3}$$

where $[\Lambda]$ and $[\Delta]$ denote the respective concentrations (*or* numbers) of Λ and Δ enantiomers present in the mixture. For a *racemic* mixture, $\eta = 0$, and for a completely resolved sample, $\eta = \pm 1$. Since absorbances are directly proportional to species (chromophore) concentrations, expressions 1 and 3 may be combined to yield

$$g_{abs}^{\eta}(\lambda) = \eta g_{abs}^{\Lambda}(\lambda) \tag{4}$$

where $g_{abs}^{\eta}(\lambda)$ is the absorption dissymmetry factor that will be observed for a mixture in which the enantiomeric excess is η, and $g_{abs}^{\Lambda}(\lambda)$ is the absorption dissymmetry factor exhibited by a sample of pure Λ enantiomers ($\eta = 1$). An expression analogous to (4) may be written for emission dissymmetry factors:

$$g_{em}^{\eta'}(\lambda') = \eta' g_{em}^{\Lambda}(\lambda') \tag{5}$$

where η' denotes enantiomeric excess *in the emitting state*, and $g_{em}^{\Lambda}(\lambda')$ is the emission dissymmetry factor characteristic of pure Λ enantiomers (emitting at wavelength λ').

Chiroptical Luminescence from a Racemic Mixture Excited with Circularly Polarized Light. If a racemic mixture of enantiomers is excited with *unpolarized* light, the excited-state population produced by the excitation will also be racemic, and no CPL will be observed from the sample. However, if a racemic mixture is excited with *circularly polarized* light, the excited-state population will be nonracemic, and CPL may be observed if the excited-state population retains at least some enantiomeric excess during the time-interval between excitation and CPL/emission detection.

Here we consider a racemic mixture of Λ and Δ enantiomers irradiated by a pulse of circularly polarized light that will produce a nonracemic population of excited-state enantiomers (Λ^* and Δ^*). The enantiomeric excess present in this excited-state population at any time (t), after the exciting light is turned off (at $t = 0$), may be written as

$$\eta_{p\lambda}^{\bullet}(t) = \frac{[\Lambda^*]_p^t - [\Delta^*]_p^t}{[\Lambda^*]_p^t + [\Delta^*]_p^t} \tag{6}$$

where p denotes the polarization of the exciting light (p = l or r for left- or right-circular polarization), λ denotes the excitation wavelength, and $[\Lambda^*]_p^t$ and $[\Delta^*]_p^t$ denote excited-state concentrations of the respective enantiomers at time t. In the initially prepared excited-state population (at $t = 0$), $[\Lambda^*]_p^0$ will be proportional to $\epsilon_p^{\Lambda}(\lambda)$, $[\Delta^*]_p^0$ will be proportional to $\epsilon_p^{\Delta}(\lambda)$, and $\eta_{p\lambda}^{\bullet}(0)$ is given by

$$\eta_{p\lambda}^{\bullet}(0) = \frac{\epsilon_p^{\Lambda}(\lambda) - \epsilon_p^{\Delta}(\lambda)}{\epsilon_p^{\Lambda}(\lambda) + \epsilon_p^{\Delta}(\lambda)} \tag{7}$$

For *left*-circularly polarized exciting light, expression 7 may be evaluated to the form:

$$\eta_{l\lambda}^{\bullet}(0) = \frac{\epsilon_l^{\Lambda}(\lambda) - \epsilon_r^{\Lambda}(\lambda)}{\epsilon_l^{\Lambda}(\lambda) + \epsilon_r^{\Lambda}(\lambda)} = \frac{\Delta\epsilon^{\Lambda}(\lambda)}{2\epsilon^{\Lambda}(\lambda)} = \frac{g_{abs}^{\Lambda}(\lambda)}{2} \tag{8}$$

where we have made use of the relation $\epsilon_l^{\Delta} = \epsilon_r^{\Lambda}$ and eq 1. For *right*-circularly polarized exciting light, $\eta_{r\lambda}^{\bullet}(0) = -\eta_{l\lambda}^{\bullet}(0)$.

In the absence of excited-state racemization processes, the enantiomers Λ^* and Δ^* will decay to their respective ground states via identical pathways, and the rate constant for each relaxation mechanism in these pathways will be identical for Λ^* and Δ^*. In this limiting case (no excited-state racemization), the initially

(18) Metcalf, D. H.; Snyder, S. W.; Wu, S.; Hilmes, G. L.; Riehl, J. P.; Demas, J. N.; Richardson, F. S. *J. Am. Chem. Soc.* **1989**, *111*, 3082-3083.

prepared enantiomeric excess, $\eta^*_{p\lambda}(0)$, will be conserved throughout the entire excited-state relaxation period. CPL/emission observed from *any* luminescent state populated during this relaxation period will exhibit a constant (time-independent) emission dissymmetry factor. If the excitation is *left*-circularly polarized (at wavelength λ) and CPL/emission is observed at wavelength λ', expressions 5 and 8 may be combined to give

$$g_{em}(\lambda') = \frac{g^{\Lambda}_{abs}(\lambda) g^{\Lambda}_{em}(\lambda')}{2} \tag{9}$$

which is the value of $2\Delta I/I = 2(I_l - I_r)/(I_l + I_r)$ that will be measured at wavelength λ'.

Racemization processes within the excited-state population introduce additional channels for Λ^* and Δ^* enantiomer relaxation. In their simplest form, these channels may be represented as follows:

$$\Lambda^* \xrightarrow{k^{\Lambda^*}_{conv}} \Delta^* \xrightarrow{k_0^{\Delta^*}} \Delta$$

$$\Delta^* \xrightarrow{k^{\Delta^*}_{conv}} \Lambda^* \xrightarrow{k_0^{\Lambda^*}} \Lambda$$

where $k^{\Lambda^*}_{conv}$ and $k^{\Delta^*}_{conv}$ denote generalized rate constants for enantiomer *interconversion* processes (within the excited-state population), and $k_0^{\Lambda^*}$ and $k_0^{\Delta^*}$ denote generalized rate constants for excited-state-to-ground-state relaxation processes. In the absence of any chiral perturbations (such as might be introduced by chiral solvent molecules or cosolutes), we may write $k^{\Lambda^*}_{conv} = k^{\Delta^*}_{conv} = k^*_{conv}$ and $k_0^{\Lambda^*} = k_0^{\Delta^*} = k_0^*$. If we adopt this simple relaxation scheme and assume that each step follows a first-order rate law, it is a relatively straightforward exercise to derive rate expressions for the enantiomer concentrations appearing in eq 6 and obtain the following expression for $\eta^*_{p\lambda}(t)$:

$$\eta^*_{p\lambda}(t) = \eta^*_{p\lambda}(0) \exp[-2k^*_{conv}t]$$
$$= \eta^*_{p\lambda}(0) \exp[-k^*_{rac}t] \tag{10}$$

where $k^*_{rac} = 2k^*_{conv}$ defines the rate constant for excited-state racemization. Combining eq 5 and 10 yields an expression for the emission dissymmetry factor:

$$g^{p\lambda}_{em}(\lambda',t) = \eta^*_{p\lambda}(0) g^{\Lambda}_{em}(\lambda') \exp[-k^*_{rac}t] \tag{11}$$

where the superscripts on g_{em} identify the excitation polarization and wavelength used to prepare the initial enantiomeric excess. If we change the pλ notation to $\lambda(+) \equiv l\lambda$ and $\lambda(-) \equiv r\lambda$ (for left- and right-circularly polarized excitation, respectively) and recall the relations $\eta^*_{l\lambda}(0) = -\eta^*_{r\lambda}(0) = g^{\Lambda}_{abs}(\lambda)/2$, then eq 11 may be reexpressed as

$$g^{\lambda(\pm)}_{em}(\lambda',t) = \pm\tfrac{1}{2} g^{\Lambda}_{abs}(\lambda) g^{\Lambda}_{em}(\lambda') \exp[-k^*_{rac}t] \tag{12}$$

Derivation of expression 10 was based on the assumption that enantiomer interconversions occur only via *first-order* rate processes, and expressions 11 and 12 require the further assumption that these rate processes are the same in all excited states sampled by the species between excitation and CPL/emission detection. The latter assumption can be avoided if excitation is *directly* into the emitting state *or* into a state that relaxes very rapidly (on the racemization time scale) to the emitting state. The assumption of first-order rate processes for enantiomeric interconversions is somewhat more problematic. However, this assumption is likely quite valid for the systems of interest in the present study. An example of a second-order rate process that might be relevant to enantiomer interconversion in these systems is nonradiative (electronic) energy transfer between opposite enantiomers:

$$\Lambda^* + \Delta \underset{k_{et}}{\overset{k_{et}}{\rightleftharpoons}} \Lambda + \Delta^*$$

The rate law for this racemization mechanism will be second-order (first-order with respect to both the ground-state and excited-state concentrations of enantiomers). However, under the usual experimental conditions, the concentrations of ground-state enantiomers far exceed those of the excited-state enantiomers, and one may assume a pseudo-first-order rate law. A more thorough and rigorous consideration of racemization via energy-transfer mechanisms has been given by Riehl and co-workers.[14]

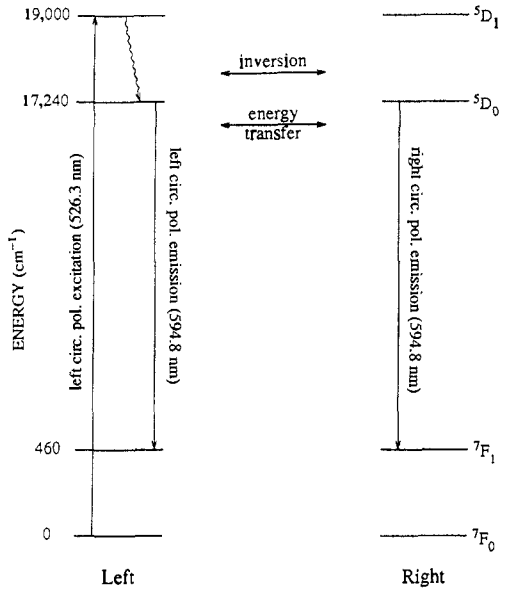

Figure 1. Excitation, emission, and kinetic scheme for the racemization of $Eu(dpa)_3^{3-}$. Here, we identify the enantiomers by their preferential emission of left- or right-circularly polarized light at 594.8 nm, as opposed to absolute (Λ or Δ) configurational stereochemical labels. Racemization of the $^5D_0$ excited-state population is shown as via energy transfer or ligand rearrangement (inversion) mechanisms. See text for details.

Applications to $Eu(dpa)_3^{3-}$. For the types of spectroscopic measurements performed in this study it is desirable to look at transitions having large dissymmetry factors. Europium(III) complexes in aqueous solution generally exhibit strong luminescence from only one multiplet of the Eu(III) $4f^6$ electronic configuration, $^5D_0$ (located at 17 250 ± 30 cm^{-1} above the ground multiplet $^7F_0$). Among the $^7F_J \leftarrow {}^5D_0$ transition manifolds represented in this luminescence, the $^7F_1 \leftarrow {}^5D_0$ manifold generally exhibits the largest emission dissymmetry factors in the CPL/emission spectra of chiral Eu(III) systems. In $Eu(dpa)_3^{3-}$, the ligand-field potential splits the $^7F_1$ multiplet into two crystal-field levels: one nondegenerate and one doubly degenerate (reflecting the trigonal dihedral (D_3) symmetry of the complex). Transitions to each of these levels are observed in emission spectra of $Eu(dpa)_3^{3-}$: one centered at ca. 590.6 nm and assigned as $A_2(^7F_1) \leftarrow A_1(^5D_0)$ and the other centered at ca. 594.8 nm and assigned as $E(^7F_1) \leftarrow A_1(^5D_0)$, where A_1, A_2, and E identify crystal-field state symmetries (appropriate for the D_3 point group). The $E \leftarrow A_1$ transition at 594.8 nm has approximately twice the intensity of the $A_2 \leftarrow A_1$ transition, and it also exhibits a larger emission dissymmetry factor. Most of the chiroptical luminescence results reported in this paper were obtained from CPL/emission measurements at 594.8 nm.

For luminescence excitation we used laser radiation at 526.3 nm. This excites the higher energy crystal-field level of the $^5D_1$ multiplet via the transition $A_1(^7F_0) \rightarrow E(^5D_1)$. The energy difference between this level and the $^5D_0$ emitting level is approximately 1770 cm^{-1}. The rate constant for the $^5D_1$ to $^5D_0$ relaxation process in $Eu(dpa)_3^{3-}$ is not known; however, for the same process in $Eu(oda)_3^{3-}$, a rate constant of 6.6×10^5 s^{-1} has been reported.[19,20] Structural isomerization processes are expected to be considerably slower, so one may assume that our measurements of excited-state racemization rates will reflect processes occurring entirely in the $^5D_0$ emitting state. Figure 1 shows the excitation, emission, and kinetic pathways for the racemization of $Eu(dpa)_3^{3-}$ in our experiments.

(19) Horrocks, W. D., Jr.; Albin, M. In *Progress in Inorganic Chemistry*; Lippard, S. Ed.; J. Wiley & Sons: New York, 1984; Vol. 31, pp 1-104.
(20) Roy, D. S.; Bhattacharayya, K.; Gupta, A. K.; Chowdury, M. *Chem. Phys. Lett.* **1981**, *77*, 422-426.

Now we reconsider expression 12, given the excitation and emission conditions cited above for $Eu(dpa)_3^{3-}$. Having specified the excitation wavelength (λ = 526.3 nm) and the emission wavelength (λ' = 594.8 nm), we suppress the λ and λ' labels in expression 12 and write

$$g_{em}^{(\pm)}(t) = [\pm{}^1/_2 g_{abs}^{\Lambda} g_{em}^{\Lambda}] \exp[-k_{rac}^{\bullet} t] = g_{em}^{(\pm)}(0) \exp[-k_{rac}^{\bullet} t] \quad (13)$$

The g_{abs}^{Λ} and g_{em}^{Λ} factors are inherent properties of pure (fully resolved) Λ - $Eu(dpa)_3^{3-}$, and they cannot be measured directly from solution. Measurements of $g_{em}^{(\pm)}(t)$ on a racemic mixture excited by left (+)- or right (−)-circularly polarized light can only provide information about the product quantity, $g_{em}^{\Lambda} g_{abs}^{\Lambda}$ (which must be identical with $g_{em}^{\Delta} g_{abs}^{\Delta}$).

In the study reported here, $g_{em}^{(\pm)}$ vs t measurements were carried out for $Eu(dpa)_3^{3-}$ in H_2O and D_2O at seven different sample temperatures between 293 and 353 K. The effects of solvent and temperature on excited-state racemization kinetics were of principal interest. However, solvent and temperature effects on the parameter, $g_{em}^{(\pm)}(0) = [\pm{}^1/_2 g_{abs}^{\Lambda} g_{em}^{\Lambda}]$ were also of some interest. This parameter reflects specific chiroptical properties characteristic of the equilibrium structures of Λ (or Δ) enantiomers in the ground ($^7F_0$) and emitting ($^5D_0$) states of $Eu(dpa)_3^{3-}$. Under the excitation and emission conditions specified above, the g_{abs}^{Λ} factor reflects the CD/absorption properties of one crystal-field component of the $^7F_0 \rightarrow {}^5D_1$ transition in europium (at 526.3 nm), and the g_{em}^{Λ} factor reflects the CPL/emission properties of a $^7F_1 \leftarrow {}^5D_0$ transition (at 594.8 nm). Small variations in $g_{em}^{(\pm)}(0)$ with solvent or temperature would imply small changes in the structure parameters of intact $Eu(dpa)_3^{3-}$ complexes, with concomitant perturbations on the relevant spectroscopic transition moments. Large variations in $g_{em}^{(\pm)}(0)$ would indicate major structure changes that might include the breakup of intact tris-chelate systems. In the latter case, $g_{em}^{(\pm)}(t)$ measurements would be of limited utility.

Finally, we consider the case where measurements of $\Delta I^{(\pm)}(t)$ and $I^{(\pm)}(t)$ are summed over all luminescence detection times. The time dependence of $I^{(\pm)}(t)$ may be expressed as

$$I(t) = I(0) \exp[-t/\tau_0] \quad (14)$$

where τ_0 denotes the luminescence lifetime of the $^5D_0$ emitting state, and the polarization ($\pm$) superscripts on I have been eliminated since the total luminescence intensity will not depend on excitation polarization. The time dependence of $\Delta I^{(\pm)}(t)$ is given by

$$\Delta I^{(\pm)}(t) = \Delta I^{(\pm)}(0) \exp\left[-\frac{t}{\tau_0} - \frac{t}{\tau_{rac}^{\bullet}}\right] \quad (15)$$

where $\tau_{rac}^{\bullet} = 1/k_{rac}^{\bullet}$ (and it is assumed that all excited-state racemization occurs in the $^5D_0$ state). Integrations of eq 14 and 15 over times long compared to τ_0 yield $\bar{I} = I(0)\tau_0$ and $\overline{\Delta I}^{(\pm)} = \Delta I^{(\pm)}(0)\tau_0\tau_{rac}^{\bullet}/(\tau_0 + \tau_{rac}^{\bullet})$, and we may define

$$\bar{g}_{em}^{(\pm)} = \frac{2\overline{\Delta I}^{(\pm)}}{\bar{I}} = \left[\frac{2\Delta I^{(\pm)}(0)}{I(0)}\right] \frac{\tau_{rac}^{\bullet}}{\tau_0 + \tau_{rac}^{\bullet}} = g_{em}^{(\pm)}(0)\left[1 + \frac{\tau_0}{\tau_{rac}^{\bullet}}\right]^{-1} = \pm{}^1/_2 g_{abs}^{\Lambda} g_{em}^{\Lambda}\left[1 + \frac{\tau_0}{\tau_{rac}^{\bullet}}\right]^{-1} \quad (16)$$

which corresponds to the emission dissymmetry factor that would be measured under steady-state (continuous) excitation/emission conditions. In the study reported here, $\overline{\Delta I}^{(\pm)}$, $\bar{I}$, and $\bar{g}_{em}^{(\pm)}$ were determined by performing time integrations over $\Delta I^{(\pm)}(t)$ and $I(t)$ decay curves.

Equation 16 may be rearranged to give

$$\Delta I^{\lambda(\pm)}(\lambda') = \pm K g_{abs}^{\Lambda}(\lambda) \bar{I}^{\lambda}(\lambda') g_{em}^{\Lambda}(\lambda') \quad (17)$$

where $K = ({}^1/_4)[1 + (\tau_0/\tau_{rac}^{\bullet})]^{-1}$, and explicit notation for excitation (λ) and emission (λ') wavelengths has been restored (vide supra). Measurements of $\overline{\Delta I}^{\lambda(\pm)}(\lambda')$ versus λ' at a fixed excitation wavelength (λ) will yield a spectrum that mimics the steady-state CPL spectrum of the pure Λ enantiomer to within a scaling factor, $\pm K g_{abs}^{\Lambda}(\lambda)$. Analogously, measurements of $\overline{\Delta I}^{\lambda(\pm)}(\lambda')$ versus λ at a fixed emission wavelength (λ') will yield a CPL excitation spectrum that mimics the circular dichroism spectrum of pure Λ to within a scaling factor, $\pm K g_{em}^{\Lambda}(\lambda')\, \bar{I}^{\lambda}(\lambda')/\epsilon(\lambda)$. In this latter scaling factor, the ratio, $\bar{I}^{\lambda}(\lambda')/\epsilon(\lambda)$, is related to relative luminescence quantum yield, and it may vary with λ. The value of K will be independent of λ so long as nonradiative relaxations to the emitting state ($^5D_0$) are fast compared to racemization processes. The upper and lower bounds on K are 0.25 (when $\tau_{rac}^{\bullet} \gg \tau_0$) and 0 (when $\tau_{rac}^{\bullet} \ll \tau_0$).

Experimental Section

A stock solution of 20 mM $Eu(dpa)_3^{3-}$ was prepared in H_2O by neutralization of dipicolinic acid with stoichiometric amounts of $Eu_2(CO_3)_3$ and Na_2CO_3 to give a [Eu]:[dpa] ratio of 1:3.5. The solution was brought to pH 8 with additional Na_2CO_3. A solution of 20 mM $Eu(dpa)_3^{3-}$ in D_2O was prepared by evaporating the H_2O of the above solution under high vacuum and dissolving the resulting solid in D_2O (Aldrich, 99.8 atom % D). The stability of the complex in solution was verified by measuring total luminescence lifetimes before and after each spectral run. In all cases, no change in TL lifetime (within experimental error) was noted.

The TR-CPL and time-resolved total luminescence (TR-TL) spectra were measured with an instrument constructed in our laboratory.[21] A N_2-laser pumped dye laser (using coumarin 540A as the dye), operating at a repetition rate of about 10 Hz, was used as the excitation source. The dye laser output was circularly polarized with a Glan-Thompson polarizer and Fresnel rhomb quarter-wave retarder. Only results obtained with left-circularly polarized light are presented in this report; excitation with right-circularly polarized light produces CPL spectra of equal magnitude but opposite sign for these systems. The sample was contained in a water-jacketed fluorescence cuvette, and the temperature was controlled to ±0.1 °C by using a circulating water bath. The sample emission was collected at a 90° angle to the excitation direction, passed through a 50-kHz photoelastic modulator and linear polarizer (which together serve as a circular polarization analyzer), and was then dispersed with a Spex 1400-II $^3/_4$-meter double-grating monochromator. The emission intensity was detected by using an EMI 9558 photomultiplier tube with S-20 response. We use a lab-built, gated photon-counting device to determine the TL and CPL content of the emission. The gates of this device are referenced to the modulation frequency of the photoelastic modulator. This device is interfaced on an AT-clone computer via a high-speed parallel interface (Metrobyte PDMA-16) which allows for the counting and transmission of CPL and TL data obtained during individual photoelastic modulator cycles. The time-resolution of this system is 20 μs, the period of one photoelastic modulator cycle. The photon-counting device triggers the firing of the laser. In order to achieve the large signal-to-noise ratios required for the observation of small TR-CPL signals, many hundreds of thousands of emission decays are summed. Each time-resolved spectrum reported in this paper represents about 18 h of data collection time. Emission and excitation spectra (as a function of wavelength) were also measured with this instrument, with the photon-counting device operating in an emission decay integration mode. The emission data was integrated over a time interval corresponding to 0.06–8 ms after the excitation pulse. (The initial delay after the excitation pulse is needed due to rf interference from the laser firing affecting the data collection.) These spectra were not corrected for either monochromator efficiency or photomultiplier response (in the case of the emission spectra) or wavelength-dependent dye laser intensity (in the excitation spectra).

Results

Time-Integrated CPL and TL. Time-integrated CPL and TL excitation spectra are shown in Figure 2 over the $^7F_0 \rightarrow {}^5D_1$ and $^7F_1 \rightarrow {}^5D_1$ transition regions of $Eu(dpa)_3^{3-}$ in D_2O at 293 K. These spectra were obtained by measuring time-integrated CPL ($\overline{\Delta I}$) and TL ($\bar{I}$) intensities at 594.8 nm, by using *left*-circularly polarized light for excitation over the wavelength range 524–541

(21) Metcalf, D. H.; Cummings, W. J.; Richardson, F. S. Manuscript in preparation.

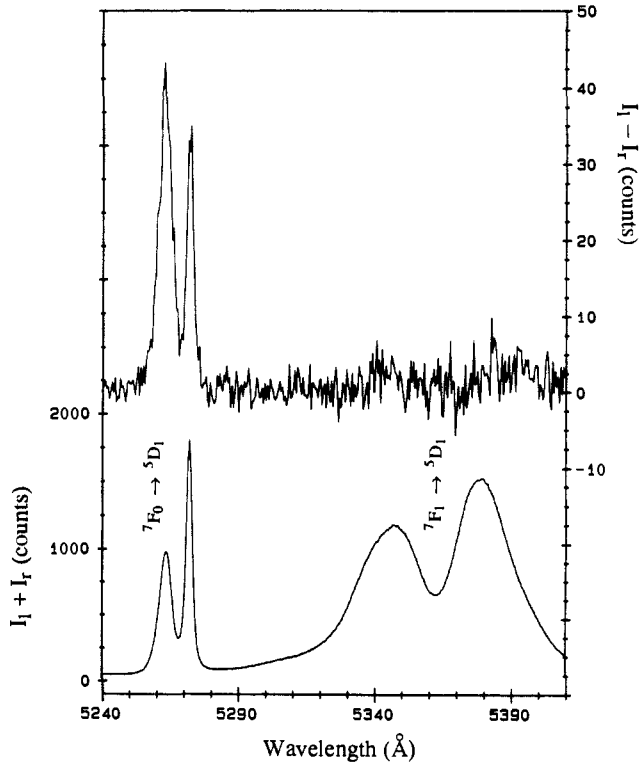

Figure 2. CPL (top, $I_l - I_r$) and TL (bottom, $I_l + I_r$) excitation spectra for 20 mM *rac*-Eu(dpa)$_3^{3-}$ in D_2O. These spectra were recorded by measuring the CPL and TL intensity at 594.8 nm (the $^7F_1 \leftarrow {}^5D_0$ transition) and scanning the left-circularly polarized dye laser through the excitation region. These spectra span the $^7F_0$, $^7F_1 \rightarrow {}^5D_1$ transition region. The spectra are not corrected for the wavelength dependence of the dye laser excitation intensity.

nm. As discussed earlier (see eq 17 and associated discussion), these spectra should qualitatively mimic the CD and absorption spectra of resolved (*either* Λ or Δ) Eu(dpa)$_3^{3-}$. More specifically, we may write

$$\frac{\overline{\Delta I}^{\lambda(+)}(\lambda')}{\bar{I}^{\lambda}(\lambda')} = [K g^{\Lambda}_{em}(\lambda')]\frac{\Delta\epsilon^{\Lambda}(\lambda)}{\epsilon(\lambda)} \qquad (18)$$

which relates the observables in our excitation spectra to the CD and absorption parameters ($\Delta\epsilon$ and ϵ) of Λ-Eu(dpa)$_3^{3-}$. The quantity shown inside square brackets will have a constant value over the $^7F_{0,1} \rightarrow {}^5D_1$ excitation region, with a sign determined by $g^{\Lambda}_{em}(\lambda')$. The $\overline{\Delta I}$ and $\bar{I}$ excitation spectra shown in Figure 2 are qualitatively identical with the CD and absorption spectra reported by Riehl and co-workers for Eu(dpa)$_3^{3-}$ in aqueous solution with the chiral cosolute (+)-dimethyl-L-tartrate present in large excess over the metal complex. In Riehl's experiments, the chiral cosolute (a "Pfeiffer reagent") produces a nonracemic equilibrium distribution of Λ- and Δ-Eu(dpa)$_3^{3-}$ enantiomers. If it is assumed that the intrinsic *spectroscopic* properties of the individual enantiomers are unaffected by the Pfeiffer reagent, then the $\Delta\epsilon(\lambda)$ and $\epsilon(\lambda)$ observables in Riehl's experiments may be related to our $\overline{\Delta I}$ and $\bar{I}$ observables by combining eq 4 and 18:

$$\frac{1}{\eta}\frac{\Delta\epsilon(\lambda)}{\epsilon(\lambda)} = [K g^{\Lambda}_{em}(\lambda')]^{-1}\frac{\overline{\Delta I}^{\lambda(+)}(\lambda')}{\bar{I}^{\lambda}(\lambda')} \qquad (19)$$

where η denotes the *ground-state* enantiomeric excess produced by the Pfeiffer reagent in Riehl's experiments.

Figure 3 shows time-integrated CPL and TL spectra over the $^7F_{0,1,2} \leftarrow {}^5D_0$ transition region of Eu(dpa)$_3^{3-}$ in D_2O at 293 K. These spectra were obtained by using *left*-circularly polarized excitation at 526.3 nm. From eq 16 and 17, we may write

$$\bar{g}^{\lambda(+)}_{em}\lambda' = \frac{2\overline{\Delta I}^{\lambda(+)}(\lambda')}{\bar{I}^{\lambda}(\lambda')} = 2K g^{\Lambda}_{abs}(\lambda) g^{\Lambda}_{em}(\lambda') \qquad (20)$$

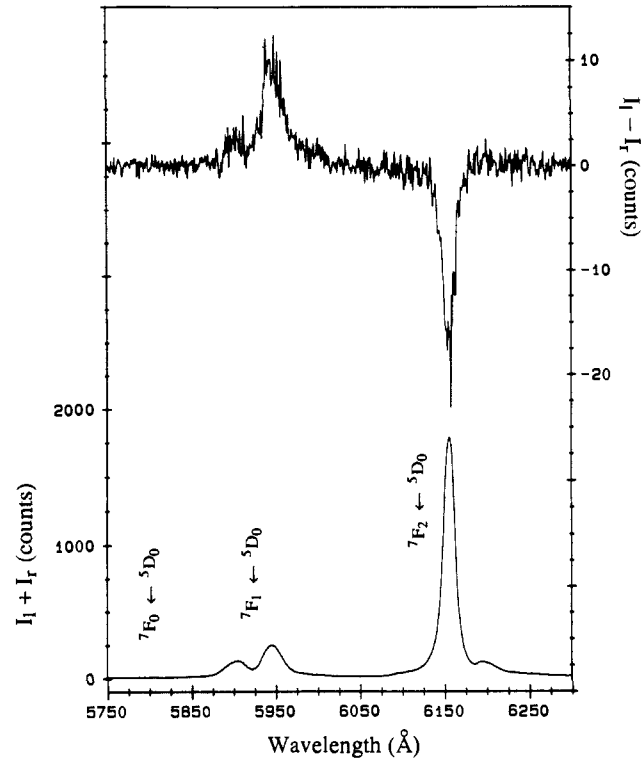

Figure 3. CPL (top, $I_l - I_r$) and TL (bottom, $I_l + I_r$) spectra for 20 mM *rac*-Eu(dpa)$_3^{3-}$ in D_2O. These spectra span the $^7F_0$, $^7F_1$, $^7F_2 \leftarrow {}^5D_0$ transition region. The sample was excited at 526.3 nm with left-circularly polarized light ($^7F_0 \rightarrow {}^5D_1$ transition). These spectra are uncorrected for monochromator or phototube response.

which relates the dissymmetry factors *observed* in our experiment to $g^{\Lambda}_{abs}(\lambda)$ and $g^{\Lambda}_{em}(\lambda')$ of the Λ enantiomer. The following values of $\bar{g}^{(+)}_{em}$ were determined for the two most intense features of the spectra shown in Figure 3: $\bar{g}^{(+)}_{em} = 8.5 \times 10^{-2}$ ($\lambda^{(+)} = 526.3$ nm, $\lambda' = 594.8$ nm) and $\bar{g}^{(+)}_{em} = -1.9 \times 10^{-2}$ ($\lambda^{(+)} = 526.3$ nm, $\lambda' = 615.7$ nm). Spectra similar to those shown in Figure 3 may be obtained from steady-state CPL/emission measurements on Eu(dpa)$_3^{3-}$ in solution with a Pfeiffer reagent. In these experiments, *unpolarized* excitation is used, and the CPL and TL observables may be denoted by $\Delta I^{\lambda(o)}(\lambda')$ and $I^{\lambda(o)}(\lambda')$. These observables may be related to those in our experiment by combining eq 5 and 20:

$$\frac{1}{\eta'}\frac{\Delta I^{\lambda(o)}(\lambda')}{I^{\lambda(o)}(\lambda')} = [2K g^{\Lambda}_{abs}(\lambda)]^{-1}\frac{\overline{\Delta I}^{\lambda(+)}(\lambda')}{\bar{I}^{\lambda}(\lambda')} \qquad (21)$$

where η' denotes the *excited-state* enantiomeric excess attributable to the Pfeiffer effect. This relationship, like eq 19, is valid only if the Pfeiffer reagent does not alter the intrinsic spectroscopic properties of the individual enantiomers.

Time-Resolved CPL and TL. Figures 4 and 5 show time-resolved CPL and TL intensities measured for Eu(dpa)$_3^{3-}$ in H_2O (Figure 4) and D_2O (Figure 5) solutions at various temperatures (expressed in °C). The luminescence was excited with *left*-circularly polarized light at $\lambda = 526.3$ nm (corresponding to a $^7F_0 \rightarrow {}^5D_1$ transition component), and the CPL and TL intensities were measured at $\lambda' = 594.8$ nm (corresponding to a $^7F_1 \leftarrow {}^5D_0$ transition component). The TL decay curves were essentially independent of temperature over the 20–80 °C range, whereas the CPL decay curves exhibit a pronounced temperature dependence. The data shown in Figures 4 and 5 were used to calculate emission dissymmetry factors, $g_{em}(t) = 2\Delta I(t)/I(t)$, and Figure 6 shows a $g_{em}(t)$ decay curve derived from the 60 °C data of Figure 5 (for Eu(dpa)$_3^{3-}$ in D_2O).

At each temperature represented in our experiments, the TL decay was well-fitted by a single-exponential function defined according to eq 14. The τ_0 parameter values obtained from such fits are listed in Table I. The τ_0 parameter exhibits very little temperature dependence in either H_2O or D_2O solution, but its values in D_2O are approximately twice those in H_2O. The $\Delta I(t)$

Table I. Kinetic, Dissymmetry, and Enantiomeric Excess Parameters from the Time-Resolved Total Luminescence and Circularly Polarized Luminescence Measurements on $Eu(dpa)_3^{3-}$ in H_2O and D_2O[a]

T (K)	k^*_{rac} (s^{-1})	τ^*_{rac} (ms)	τ_0 (ms)	τ_{CPL} (ms)	$g^{(+)}_{em}(0) \times 10^2$	$\bar{g}^{(+)}_{em} \times 10^2$	$\bar{\eta}^{(+)}/g^{\Lambda}_{abs}$
			H_2O				
293.2	31.7 ± 5.0	31.6 ± 5.0	1.6138 ± 0.0011	1.541 ± 0.012	8.50 ± 0.10	8.09 ± 0.42	0.477
303.2	56.6 ± 4.4	17.7 ± 1.4	1.6022 ± 0.0013	1.477 ± 0.010	8.15 ± 0.08	7.47 ± 0.32	0.461
313.2	114.9 ± 5.1	8.70 ± 0.39	1.5976 ± 0.0007	1.353 ± 0.010	7.88 ± 0.07	6.66 ± 0.36	0.423
323.2	196.5 ± 7.5	5.09 ± 0.19	1.5936 ± 0.0008	1.218 ± 0.011	7.58 ± 0.08	5.77 ± 0.28	0.382
333.2	360.8 ± 14.2	2.77 ± 0.11	1.5864 ± 0.0009	1.012 ± 0.015	7.21 ± 0.11	4.58 ± 0.25	0.319
343.2	520.9 ± 14.3	1.92 ± 0.05	1.5821 ± 0.0006	0.871 ± 0.011	6.43 ± 0.08	3.53 ± 0.24	0.275
353.2	899.7 ± 33.3	1.11 ± 0.04	1.5757 ± 0.0005	0.655 ± 0.014	4.68 ± 0.10	1.93 ± 0.11	0.208
			D_2O				
293.2	22.0 ± 1.4	45.5 ± 3.0	3.1935 ± 0.0009	2.988 ± 0.013	9.15 ± 0.04	8.55 ± 0.14	0.468
303.2	45.7 ± 1.5	21.9 ± 0.7	3.1914 ± 0.0014	2.792 ± 0.012	8.95 ± 0.05	7.82 ± 0.30	0.437
313.2	83.8 ± 2.1	11.9 ± 0.3	3.1733 ± 0.0020	2.514 ± 0.013	8.77 ± 0.05	6.93 ± 0.21	0.396
323.2	154.8 ± 3.3	6.46 ± 0.14	3.1663 ± 0.0031	2.130 ± 0.015	8.56 ± 0.06	5.74 ± 0.16	0.336
333.2	259.5 ± 4.6	3.85 ± 0.07	3.1519 ± 0.0026	1.739 ± 0.014	7.96 ± 0.07	4.38 ± 0.12	0.276
343.2	449.0 ± 11.4	2.23 ± 0.06	3.1495 ± 0.0034	1.308 ± 0.019	7.46 ± 0.11	3.09 ± 0.13	0.208
353.2	695.7 ± 22.3	1.44 ± 0.05	3.1402 ± 0.0034	0.989 ± 0.021	6.78 ± 0.14	2.13 ± 0.12	0.157

[a] See text for full description.

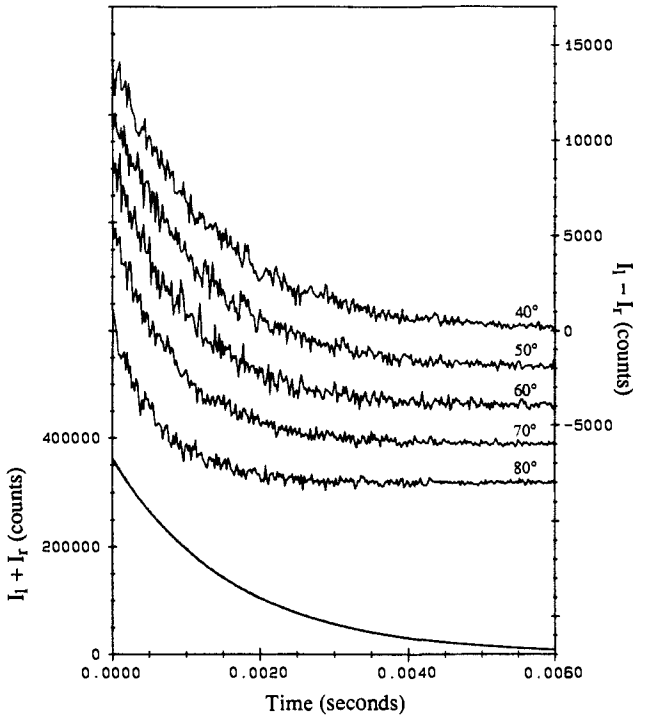

Figure 4. Time-resolved CPL (top noisy traces, $I_l - I_r$) and TL (bottom smooth trace, $I_l + I_r$) for 20 mM *rac*-$Eu(dpa)_3^{3-}$ in H_2O at various temperatures. These spectra were excited with left-circularly polarized light at 526.3 nm (the $^7F_0 \rightarrow {}^5D_1$ transition), and the emission was recorded at 594.8 nm ($^7F_1 \leftarrow {}^5D_0$ transition). All the TL spectra are overlayed, while each CPL spectrum is offset by 2000 counts on the CPL axis.

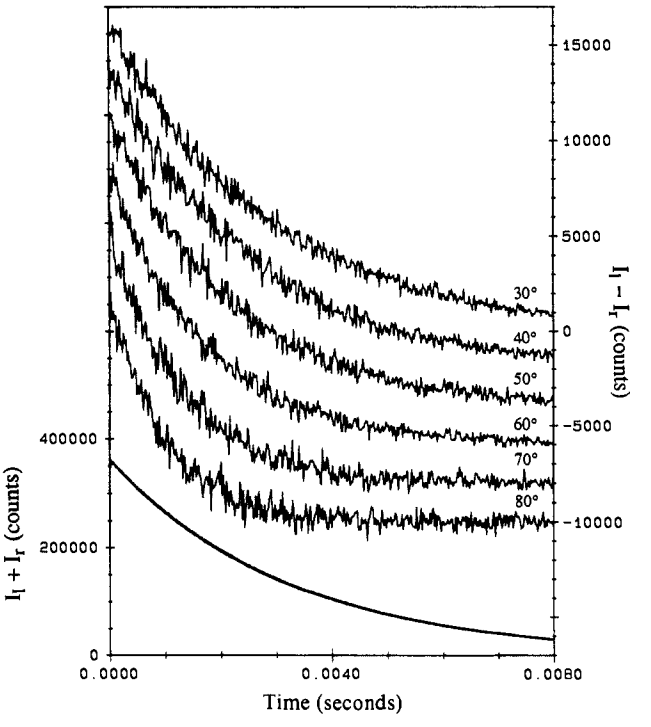

Figure 5. Time-resolved CPL (top noisy traces, $I_l - I_r$) and TL (bottom smooth trace, $I_l + I_r$) for 20 mM *rac*-$Eu(dpa)_3^{3-}$ in D_2O at various temperatures. See Figure 3 for experimental details.

and $g_{em}(t)$ decay curves were also well-fitted by single-exponential functions given by eq 15 and 13, respectively. The emission dissymmetry data were actually fitted to the equation

$$g^{(+)}_{em}(t) = g^{(+)}_{em}(0) \exp[-k^*_{rac}t] \times \frac{I(t) - dc}{I(t)} \qquad (22)$$

using a Poisson-weighted nonlinear least-squares fitting method.[22] This equation is equivalent to eq 13, with the last factor providing a correction for the offset created by dark counts (dc) in the TL data. An example of a data fit to eq 22 is given in Figure 6. The $g^{(+)}_{em}(0)$ and k^*_{rac} parameter values obtained from fits of emission dissymmetry factor data to eq 22 are summarized in Table I. Unlike τ_0, both $g^{(+)}_{em}(0)$ and k^*_{rac} exhibit a solvent *and* temperature dependence over the 20–80 °C range. All standard deviations listed in Table I were calculated according to the methods of Bevington.[23]

Table II. Activation Parameters for the Racemization of $Eu(dpa)_3^{3-}$ in H_2O and D_2O

	H_2O	D_2O
E_a (kcal/mol)	11.3 ± 0.2	11.7 ± 0.1
ln (A) (A in s^{-1})	22.2 ± 0.3	22.6 ± 0.2
$\Delta H^{\ddagger}$ (kcal/mol)	10.6 ± 0.2	11.1 ± 0.1
$\Delta S^{\ddagger}$ (cal/K-mol)	−16.7 ± 0.7	−15.7 ± 0.4

Table I also lists values determined for the following quantities: CPL lifetimes (τ_{CPL}), from fits of the time-dependent CPL data to eq 15, where we define $(1/\tau_{CPL}) = (1/\tau_0) + (1/\tau^*_{rac})$; $\bar{g}^{(+)}_{em}$, defined according to eq 16; and $\bar{\eta}^{(+)}$, which is defined by $\bar{\eta}^{(+)} = (1/2)(\tau_{CPL}/\tau_0)\bar{g}^{\Lambda}_{abs}$. The latter quantity corresponds to the "time-average" enantiomeric excess in the emitting state, and it

(22) O'Connor, D. V.; Phillips, D. *Time-Correlated Single Photon Counting*; Academic Press: New York, 1984. Marquardt, D. W. *J. Soc. Ind. Appl. Math* **1963**, *11*, 431.

(23) Bevington, P. R. *Data Reduction and Error Analysis for the Physical Sciences*; McGraw-Hill: New York, 1969.

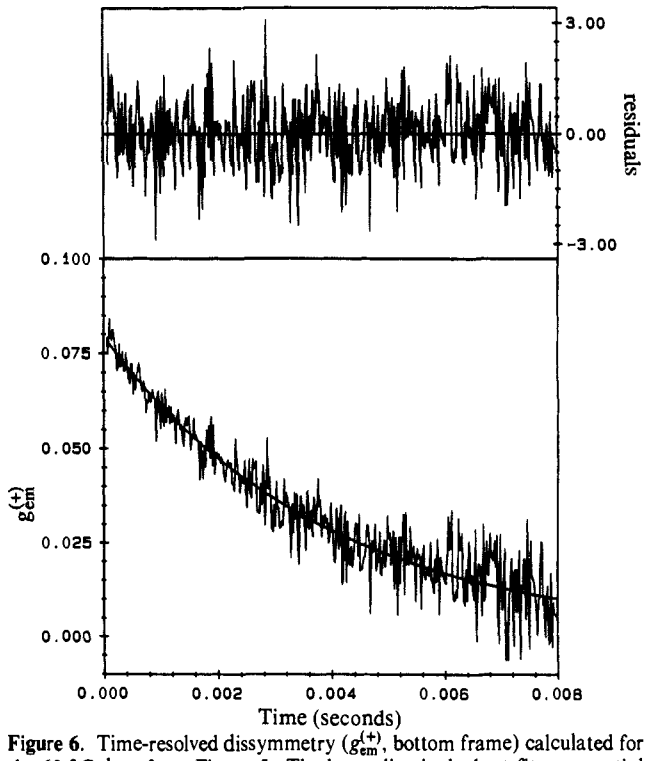

Figure 6. Time-resolved dissymmetry ($g_{em}^{(+)}$, bottom frame) calculated for the 60 °C data from Figure 5. The heavy line is the best-fit exponential curve calculated from eq 22 in the text, with $g_{em}^{(+)}(0) = 7.96 \times 10^2$ and $k_{rac}^{*} = 259.5\ s^{-1}$. The top frame shows the weighted error residuals.

relates $\bar{g}_{em}^{(+)}$ to g_{em}^{A} according to $\bar{g}_{em}^{(+)} = \bar{\eta}^{(+)} g_{em}^{A}$. Expressed in terms of the K parameter (introduced in eq 17), this enantiomeric excess is given by $\bar{\eta}^{(+)} = 2Kg_{abs}^{A}$, which is identical with the quantity shown inside square brackets on the right-hand side of eq 21.

The parameter of interest for kinetics analysis is $k_{conv}^{*} = {}^{1}/_{2}k_{rac}^{*}$, which is the rate constant for enantiomer *interconversion* processes in the emitting state ($^5D_0$) (vide supra). Plots of ln (k_{conv}^{*}) versus T^{-1} yield values for the Arrhenius parameters (E_a and A) as listed in Table II. Plots of ln (k_{conv}^{*}/T) versus T^{-1} are shown in Figure 7. These plots were used to determine activation enthalpies($\Delta H^{\ddagger}$) and entropies ($\Delta S^{\ddagger}$) according to

$$\ln\left[\frac{k_{conv}^{*}}{T}\right] = \ln\left[\frac{k_B}{h}\right] + \frac{\Delta S^{\ddagger}}{R} - \frac{\Delta H^{\ddagger}}{RT} \qquad (23)$$

where k_B is the Boltzmann constant, h is the Planck constant, and R is the gas constant. The values derived for $\Delta H^{\ddagger}$ and $\Delta S^{\ddagger}$ are given in Table II, and plots of eq 23 using these values are shown as solid lines in Figure 7.

Discussion

Structural Species in Solution. The single-exponential decay behavior observed for both CPL and TL throughout the 293–353 K temperature range provides strong evidence that only one type of Eu(III) *chemical* species is present at a detectable concentration level in the solution samples examined in this study. This confirms previous work on similarly constituted samples showing that only intact $Eu(dpa)_3^{3-}$ complexes should be present in significant concentration.[12,24] The existence of these complexes as a *racemic* mixture of structural enantiomers (in aqueous solution under ground-state equilibrium conditions) is demonstrated by the chiroptical measurements reported here and in previous work.[10,16] In solution, $Eu(dpa)_3^{3-}$ exhibits no circular dichroism in its absorptive transitions, and no circularly polarized intensity differentials ($\Delta I = I_l - I_r$) are observed in luminescence excited by *unpolarized* light. However, circularly polarized intensity differentials are observed in luminescence excited by *circularly polarized* light, with left- and right-circularly polarized excitation

(24) Grenthe, I. *J. Am. Chem. Soc.* **1961**, *83*, 360–364.

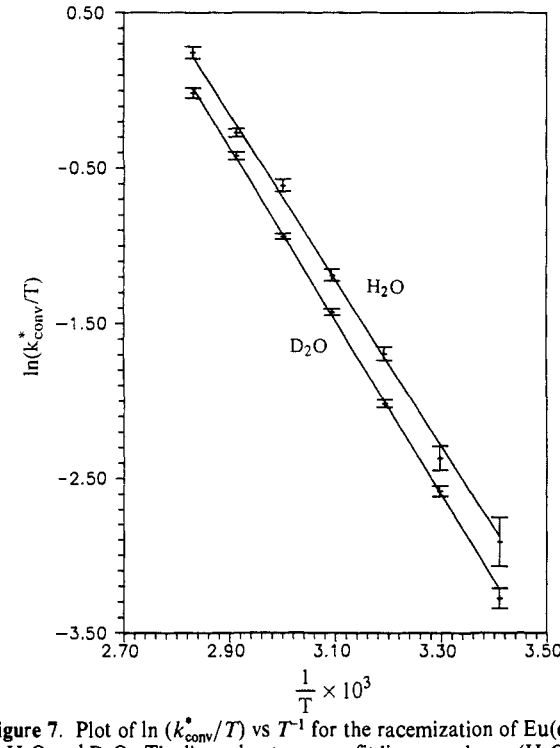

Figure 7. Plot of ln (k_{conv}^{*}/T) vs T^{-1} for the racemization of $Eu(dpa)_3^{3-}$ in H_2O and D_2O. The linear least-squares fit lines are shown (H_2O, slope -5349.0, intercept 15.36; D_2O, slope -5591.4, intercept 15.85.

(of like wavelength and intensity) producing ΔI values that are equal in magnitude but opposite in sign at any given emission wavelength. These observations reflect a racemic mixture of $Eu(dpa)_3^{3-}$ enantiomers in solution under ground-state equilibrium conditions. Previously reported spectroscopic and structural studies of $Eu(dpa)_3^{3-}$ in solution[7] and in crystals[1,2] suggest that these enantiomers have trigonal-dihedral (D_3) symmetry with either left-handed (Λ) or right-handed (Δ) configurational chirality about their 3-fold symmetry axis. This view is entirely compatible with the spectroscopic results obtained in the present study.

The structures described above may be presumed to represent the thermodynamically most stable structures of $Eu(dpa)_3^{3-}$ in the ground state *and* in the excited electronic states relevant to this study. The excited states probed in our experiments involve excitations *within* the $4f^6$ electronic configuration of Eu(III), and, to a very good approximation, one may assume that their stereochemical properties will be identical with those of the ground state. However, it is important to keep in mind that our experimental measurements monitor excited-state populations in which enantiomer interconversions occur during the periods of observation. If these interconversions occur via an intramolecular isomerization mechanism, the complexes must pass through an *achiral* transition-state structure, but the intermediate structures formed along the isomerization pathway need not have the same symmetry as either the stable isomers (D_3) or the transition state. Our results show no *direct* evidence that transient intermediate structures contribute to our spectroscopic observables.

Luminescence Lifetimes and Dissymmetry Factors. The TL lifetimes (τ_0) measured for $Eu(dpa)_3^{3-}$ in H_2O and D_2O exhibit very little temperature dependence over the 293–353 K temperature range (see Table I). This invariance reflects the constitutive stability of the complex with respect to solvent-ligand exchange. However, the lifetimes observed for D_2O solutions are approximately twice as long as those observed for H_2O solutions. It is unlikely that solvent molecules occupy inner-sphere coordination sites in "hydrated" $Eu(dpa)_3^{3-}$ complexes, but it is highly likely that they form reasonably strong hydrogen (or deuterium) bonds with the six carboxylate donor moieties in $Eu(dpa)_3^{3-}$. This view is supported by X-ray crystallographic analyses reported for $Na_3[Ln(dpa)_3]\cdot nH_2O$ compounds.[1,2] The waters of hydration attached to $Eu(dpa)_3^{3-}$ via hydrogen bonding to the carboxylate groups would be expected to exert a nonnegligible influence on

the ligand field sensed by the Eu(III) 4f electrons and thereby affect the radiative and nonradiative transition probabilities that govern τ_0, the lifetime of the $^5D_0$ emitting state. Both direct and indirect interaction mechanisms can contribute to solvent effects on τ_0, but the mechanisms may differ with respect to their differentiation between H_2O and D_2O. Relative O–H *versus* O–D oscillator frequencies (within H_2O and D_2O molecules) are likely to be most important in the *direct* interaction mechanisms, whereas relative H- *versus* D-bonding strengths are likely to be most important in the *indirect* mechanisms. The mechanistic bases of solvent effects on τ_0 are of no immediate importance in the present study. However, they are not entirely unrelated to the more important issue of solvent effects on Eu(dpa)$_3^{3-}$ racemization kinetics (vide infra).

The CPL lifetimes (τ_{CPL}) exhibit both solvent and temperature dependence over the 293–353 K temperature range. They differ significantly from TL lifetimes (τ_0) at the higher temperatures in this range, but they approach the τ_0 values at 293 K for both H_2O and D_2O solutions. In our experiments, both CPL and TL are measured after enantioselective excitation of *racemic*-Eu(dpa)$_3^{3-}$ with *left*-circularly polarized light. This excitation produces a *nonracemic* excited-state population of enantiomers in which $[\Lambda^*] \neq [\Delta^*]$. Time-resolved CPL measurements monitor $[\Lambda^*] - [\Delta^*]$ as a function of time (after excitation), whereas time-resolved TL measurements monitor $[\Lambda^*] + [\Delta^*]$ as a function of time. In the absence of excited-state enantiomer interconversion processes, the CPL and TL decay rates will be identical, and the values of τ_{CPL} and τ_0 will be the same. In the presence of excited-state enantiomer interconversion processes, the relationship between τ_{CPL} and τ_0 may be written as

$$\frac{1}{\tau_{CPL}} = \frac{1}{\tau_0} + 2k^*_{conv} \tag{24}$$

where k^*_{conv} denotes a first-order rate constant for $\Lambda^* \rightleftharpoons \Delta^*$ interconversion processes (vide supra). The temperature dependence observed in our measurements of τ_{CPL} can be attributed almost entirely to temperature dependence in k^*_{conv}, whereas both τ_0 and k^*_{conv} contribute to the solvent dependence observed for τ_{CPL}.

The time-resolved emission dissymmetry data provide a direct measure of k^*_{conv} (see eq 22 in which $k^*_{rac} = 2k^*_{conv}$), and the temperature dependence of these data may be analyzed in terms of kinetic activation parameters for Λ^*-Eu(dpa)$_3^{3-} \rightleftharpoons \Delta^*$-Eu(dpa)$_3^{3-}$ isomerization processes in H_2O and D_2O (see eq 23, Figure 7 and Table II). The activation parameters and possible mechanisms governing these isomerization processes will be discussed in a subsequent section of this paper. The time-resolved emission dissymmetry measurements also yield values for $g^{(+)}_{em}(0)$, the *initial* dissymmetry factor observed in the $^7F_1 \leftarrow {}^5D_0$ luminescence at $\lambda' = 594.8$ nm (when excitation is with *right*-circularly polarized light at $\lambda = 526.3$ nm). In our earlier discussion of theory, we showed that the *limiting* value of $g^{(+)}_{em}(0)$ is given by $(^1/_2)g^{\Lambda}_{abs}(\lambda)g^{\Lambda}_{em(\lambda')}$, which depends only on inherent chiroptical properties of resolved Eu(dpa)$_3^{3-}$. Expressed in terms of transition rotatory strengths and dipole strengths, this limiting value of $g^{(+)}_{em}(0)$ is given by

$$g^{(+)}_{em}(0) = (^1/_2)\left[\frac{4\chi_a R^{\Lambda}_a}{D_a}\right]\left[\frac{4\chi_e R^{\Lambda}_e}{D_e}\right]$$

$$= 8\chi_a\chi_e\left[\frac{R^{\Lambda}_a R^{\Lambda}_e}{D_a D_e}\right] \tag{25}$$

where R^{Λ}_a and R^{Λ}_e denote rotatory strengths, and D_a and D_e denote dipole strengths, for the absorptive (a) and emissive (e) transitions occurring at $\lambda = 526.3$ nm and $\lambda' = 594.8$ nm, respectively. The χ_a and χ_e factors correct for sample refractivity effects on the spectroscopic absorption and emission processes.

Our measured values of $g^{(+)}_{em}(0)$ should correspond to limiting values under conditions in which $^5D_1$ to $^5D_0$ excited-state relaxation is fast compared to enantiomer interconversion processes (vide supra). It is likely that these conditions are met in all of our experiments. Therefore, observed variations in $g^{(+)}_{em}(0)$ with temperature and solvent (see Table I) can be attributed to temperature and solvent effects on the spectroscopic parameters appearing in eq 25. Among these parameters, the transition rotatory strengths are expected to be most sensitive to environmental effects on ligand structure and 4f-electron/ligand-field interactions. Our measured values of $g^{(+)}_{em}(0)$ indicate substantial temperature and solvent effects on the *inherent* chiroptical properties of Eu(dpa)$_3^{3-}$ complexes in solution, but all of our measurements are compatible with the earlier assertion that these complexes exist in just two (stable) structural forms, Λ-Eu(dpa)$_3^{3-}$ and Δ-Eu(dpa)$_3^{3-}$, each with D_3 symmetry.

The $\bar{g}^{(+)}_{em}$ values listed in Table I reflect the solvent and temperature dependence of $g^{(+)}_{em}(0)$, τ_0, and τ^*_{rac} ($=1/k^*_{rac}$), and they correspond to the emission dissymmetry factors that would be measured under steady-state (continuous) excitation/emission conditions. The $\bar{\eta}^{(+)}$ quantities in Table I give the "time-average" enantiomeric excess in the emitting state ($^5D_0$), and they are defined according to

$$\bar{\eta}^{(+)} = (^1/_2)\left[\frac{\tau_{CPL}}{\tau_0}\right]g^{\Lambda}_{abs}(\lambda) \tag{26}$$

From the data presented in this paper, we cannot determine a value for $g^{\Lambda}_{abs}(\lambda)$ for Λ-Eu(dpa)$_3^{3-}$. However, from chiral-quenching experiments of Eu(dpa)$_3^{3-}$ with *resolved* Co(en)$_3^{3-}$ (en ≡ 1,2-ethanediamine) in D_2O at 20 °C, we have determined a limiting emission dissymmetry *magnitude*, $|g^{\Lambda(\Delta)}_{em}(\lambda')|$, at $\lambda' = 594.8$ nm of 0.13 for enantiomerically resolved Eu(dpa)$_3^{3-}$. As has been described in an earlier communication,[18] it is possible to produce an excited-state enantiomeric excess via enantioselective quenching of a racemic excited-state population by a resolved quenching reagent. In order to determine $|g^{\Lambda(\Delta)}_{em}(\lambda')|$, we create an initial enantiomeric excess in the excited-state population of Eu(dpa)$_3^{3-}$ through excitation with circularly polarized light and then further enhance that enantiomeric excess by selectively quenching the other enantiomer with the resolved quencher, present in a very small amount (10 μM). Time-resolved measurements show that the dissymmetry magnitude increases rapidly to a limiting value of $|g^{\Lambda(\Delta)}_{em}(\lambda')| = 0.13$. Use of this value in expression 9, along with the measured value of $\bar{g}^{(+)}_{em}$ ($\lambda^{(+)} = 526.3$ nm, $\lambda = 594.8$ nm) of 8.5×10^{-2} (vide supra) gives a value of 1.3 for $|g^{\Lambda}_{abs}(\lambda)|$, where $\lambda = 526.3$ nm. Assuming that this value does not change with temperature or between D_2O and H_2O, we can then calculate values for the time-averaged enantiomeric excess produced from excitation with circularly polarized light at $\lambda = 526.3$ nm, by using expression 26 above and the values of $\bar{\eta}^{(+)}/g^{\Lambda}_{abs}$ in the last column of Table I. The magnitudes of $|\bar{\eta}^{(+)}|$ range from 0.62 and 0.61 at 20 °C in H_2O and D_2O, respectively, to 0.27 and 0.20 at 80 °C in H_2O and D_2O, respectively. In light of the temperature and solvent dependence noted above for $g^{(+)}_{em}(0)$ and $\bar{g}^{(+)}_{em}$ (Table I), our above assumption may not be valid, and so these values should be considered approximate, especially for the higher temperatures.

Racemization Kinetics and Mechanisms. The phenomenological rate constant defined for excited-state racemization processes, k^*_{rac}, exhibits both solvent and temperature dependence (see Table I). The temperature-dependent rate data obtained for both H_2O and D_2O solutions are fitted quite satisfactorily by the two-parameter expression 23, yielding the activation enthalpies ($\Delta H^{\ddagger}$) and entropies ($\Delta S^{\ddagger}$) listed in Table II. Over the temperature range investigated in this study, the racemization rate data are similarly well-fitted by the Arrhenius equation, $k^*_{conv} = (^1/_2)k^*_{rac} = A\exp[-E_a/RT]$, yielding the A and E_a parameter values given in Table II. The kinetic parameters listed in Table II have similar values for H_2O and D_2O solutions, but there are small, statistically significant, quantitative differences that suggest solvent isotope effects on the racemization kinetics.

Earlier in this report, two general types of racemization mechanisms were discussed briefly. One type involves stereochemical rearrangement of the dpa ligands about the europium ion, and the other type involves electronic energy transfer between

ground-state and excited-state $Eu(dpa)_3^{3-}$ enantiomers of *opposite* handedness. The energy-transfer mechanism requires no ligand motions, but it does require interactions between the 4f-electron distributions on two different $Eu(dpa)_3^{3-}$ complexes. These negatively charged complexes are unlikely to experience close encounters in dilute solution, so any interactions between their 4f-electron distributions would have to be relatively long-range. This precludes interaction mechanisms based on orbital overlap and suggests consideration of energy transfer via *electrostatic* coupling between resonant 4f–4f transition dipoles. Under the conditions employed in our experiments, the energy donor complexes exist in either $^5D_0$ or $^5D_1$ excited states, and the acceptor complexes are thermally distributed among $^7F_0$, $^7F_1$, and $^7F_2$ states. The $^7F_0 \leftrightarrow {}^5D_0$ transitions are electric- *and* magnetic-dipole forbidden (in D_3 symmetry), and the $^7F_0 \leftrightarrow {}^5D_1$ and $^7F_1 \leftrightarrow {}^5D_0$ transitions are predicted to be almost entirely magnetic-dipole in character and, therefore, not subject to significant electrostatic coupling. The only transitions suitable for contributing to energy transfer via an electric dipole–electric dipole coupling mechanism are $^7F_1 \leftrightarrow {}^5D_1$, $^7F_2 \leftrightarrow {}^5D_0$, and $^7F_2 \leftrightarrow {}^5D_1$. However, over the temperature range represented in this study, the fraction of acceptor complexes in a $^7F_1$ level would be less than 25%, and the fraction in a $^7F_2$ level would be less than 3%. Furthermore, as was noted earlier, the lifetime of the $^5D_1$ state (in the donor complexes) is expected to be very short.

The discussion given above suggests the absence of efficient energy-transfer pathways between $Eu(dpa)_3^{3-}$ complexes in solution and argues against an energy-transfer mechanism for racemization. Stereochemical rearrangements provide more probable mechanistic pathways for racemization. In general, these pathways may be characterized as *either* (1) entirely intramolecular with no dissociation of the dpa ligands *or* (2) partially intramolecular with some exchange between solvent molecules and ligand donor groups at one or more coordination sites.[25] Previous studies of Eu(III)–dipicolinate complexes in aqueous solution have shown that dpa–H_2O exchange rates are slow on the time scale of $^5D_0$ luminescence.[12,13] Therefore, racemization occurring via a ligand dissociation–reassociation mechanistic pathway would not be observed in our experiments, and we may focus on intramolecular mechanisms in which all three dpa ligands of a $Eu(dpa)_3^{3-}$ complex remain in the inner-coordination sphere during enantiomer interconversion processes.

Two nondissociative intramolecular racemization mechanisms have been described in the literature for chiral, *tris-bidentate* transition-metal complexes.[26] These complexes differ from $Eu(dpa)_3^{3-}$ with respect to coordination number (six versus nine), shape of coordination polyhedra (trigonal antiprism versus tricapped trigonal prism), and ligand denticity (bidentate versus terdentate). However, their stereochemical properties are closely similar to those of $Eu(dpa)_3^{3-}$ with respect to configurational chirality and chelate ring distribution about the metal ion. In each case, the chelate rings form a three-bladed propeller structure with either left-handed (Λ) or right-handed (Δ) chirality about a 3-fold (C_3) symmetry axis. Each monocyclic chelate ring in the *tris-bidentate* transition-metal complexes has a 2-fold (C_2) symmetry axis, and each bicyclic chelate ring in *tris-terdentate* $Eu(dpa)_3^{3-}$ also has a C_2 symmetry axis. We propose here that the intramolecular mechanistic pathways for enantiomer interconversion in $Eu(dpa)_3^{3-}$ can be viewed as closely analogous to those proposed earlier for chiral, tris-bidentate transition-metal complexes. These mechanistic pathways are often referred to as the *trigonal-twist* (or Bailar) mechanism and the *rhombic-twist* (or Ray–Dutt) mechanism.

The trigonal-twist mechanism involves a *concerted* twist (or partial rotation) of *all three* chelate rings about their C_2 axes. This mechanism converts one enantiomer into the other along an isomerization pathway that passes through an *achiral* transition state of D_{3h} symmetry. The rhombic-twist mechanism involves

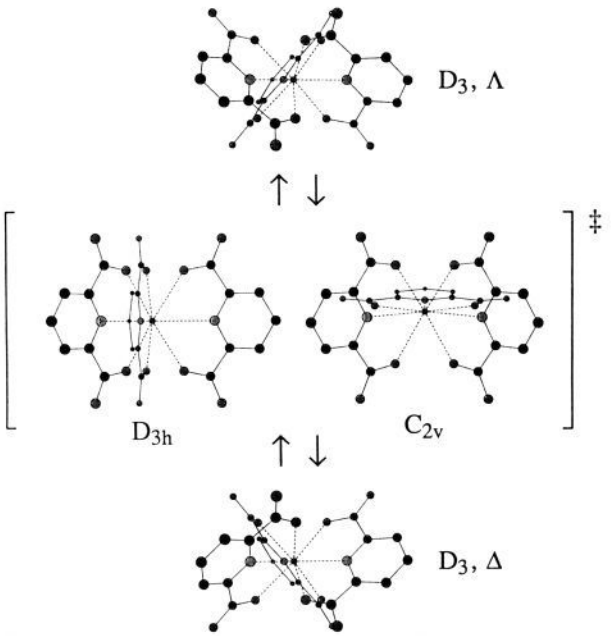

Figure 8. Proposed intramolecular mechanisms for the racemization of $Eu(dpa)_3^{3-}$. Transition states for both the trigonal-twist (Bailar) mechanism (left) and rhombic-twist (Ray–Dutt) mechanism (right) are shown. The coordinates for the chiral top and bottom structures were taken from a crystal structure of $Yb(dpa)_3^{3-}$ reported in ref 2, and the coordinates for the achiral transition states were calculated by rotating the appropriate ligands and translating them away from the central Eu^{3+} ion by an arbitrary amount.

the twisting of just *two* chelate rings (as a unit) about the C_2 axis of the third ring in the complex. The isomerization pathway in this mechanism passes through an *achiral* transition state of C_{2v} symmetry. Structures for the proposed D_{3h} and C_{2v} transition states *and* for the $\Lambda(D_3)$ and $\Delta(D_3)$ enantiomers of $Eu(dpa)_3^{3-}$ are depicted in Figure 8. Both the trigonal-twist and rhombic-twist isomerization mechanisms provide plausible pathways for Λ-$Eu(dpa)_3^{3-} \rightleftharpoons \Delta$-$Eu(dpa)_3^{3-}$ enantiomer interconversions, but our experimental results give no direct evidence or clues regarding which mechanism might be dominant.

Rodger and Johnson have developed a semiquantitative model which they used to predict the stabilities of transition states for ML_n isomerization reactions.[27] Their model assumes that transition-state stability is related to the degree of distortion (or stretching) of M–L bonds as well as to the amount of repulsion between different ligating atoms. For tris-bidentate D_3 complexes, they found that, in complexes where the chelate bite distance is large compared to the distance between closest ligating atoms of different ligands, the rhombic-twist (C_{2v}) transition state is lower in energy than the trigonal-twist (D_{3h}) transition state. For our $Eu(dpa)_3^{3-}$ complex, using distances from the crystal structure of the $Yb(dpa)_3^{3-}$ complex,[2] the chelate bite distance (the distance between the ligating carboxylate oxygens of a dpa ligand) is about 4.28 Å, while the distance between closest ligating oxygens of adjacent dpa ligands is about 2.51 Å. Thus, according to the Rodger–Johnson model,[27] the C_{2v} transition state (Figure 8) is lower in energy than the D_{3h} transition state, and the racemization occurs via the rhombic-twist mechanism. We note, however, that external interactions (e.g., solvent interactions) as well as specific details of lanthanide-ligand coordination are not considered in this model, and, therefore, conclusions based on the Rodger–Johnson model remain somewhat speculative.

Both of the transition states shown in Figure 8 are larger than the equilibrium-state structures, and their formation in solution would require significant disruption of solvent structure. Furthermore, it is likely that each would entail some alterations in the *specific* interactions between dpa carboxylate groups and

(25) Basolo, F.; Pearson, R. G. *Mechanisms of Inorganic Reactions*, 2d ed.; John Wiley and Sons: New York, 1967; Chapter 4.
(26) Minor, S. S.; Everett, G. W., Jr. *Inorg. Chem.* **1976**, *15*, 1526–1530.
(27) Rodger, A.; Johnson, B. F. G. *Inorg. Chem.* **1988**, *27*, 3061–3062.

solvent molecules. Each of these considerations regarding transition-state formation would contribute to the solvent dependence exhibited by the kinetic activation parameters listed in Table II. Both mass effects and relative hydrogen-bonding versus deuterium-bonding energies (and structure)[28] are likely contributors to the different rates of racemization observed for $Eu(dpa)_3^{3-}$ in H_2O versus D_2O solutions.

Conclusion

This is the first report of time-resolved circularly polarized luminescence (TR-CPL) from a racemic mixture of enantiomeric species excited with circularly polarized light. It is also the first report of kinetic parameters for optical isomerization of a chiral lanthanide complex. Enantioselective TR-CPL measurements provide an excellent diagnostic probe of excited-state chiroptical properties in systems that exhibit stereochemical lability on a time scale comparable to luminescence decay. In the present study, TR-CPL measurements were used to investigate the kinetics of enantiomer interconversion processes in enantioselected excited-state populations of $Eu(dpa)_3^{3-}$ in H_2O and D_2O. The results reported here are specific to $Eu(dpa)_3^{3-}$, but they also have relevance to stereochemical lability in other metal complexes.

Acknowledgment. This work was supported by grants from the National Science Foundation (CHE-8820180 to F.S.R. and CHE-8817809 to J.N.D.). We also gratefully acknowledge several helpful discussions with Dr. James P. Riehl and Dr. Gary L. Hilmes (University of Missouri-St. Louis) and essential technical assistance from William J. Cummings on instrumentation design.

(28) Kuharski, R. A.; Rossky, P. J. *J. Chem. Phys.* **1985**, *82*, 5164-5177.

The One-Electron Reduction Potential of 4-Substituted Phenoxyl Radicals in Water

J. Lind, X. Shen, T. E. Eriksen, and G. Merényi*

Contribution from the Departments of Nuclear and Physical Chemistry, Royal Institute of Technology, S-10044 Stockholm, Sweden. *Received May 31, 1989*

Abstract: By means of pulse radiolysis the one-electron reduction potentials of twelve 4-substituted phenoxy radicals have been determined. The main reference used was the $ClO_2^{\bullet}/ClO_2^-$ couple. By combining the redox potentials of phenoxyl radicals with the aqueous acidities of phenols the bond strength of the phenolic O–H bond was calculated. These values were found to be in good agreement with O–H bond dissociation enthalpies measured in the gas phase.

Phenols are of special interest in organic chemistry in that their acid–base equilibria are often used as reference values in establishing linear free energy relationships. Consequently, much effort has been expended in the past to understand the factors governing phenol acidities both in solution[1,2] and in the gas phase.[3,4] Much less is known about the redox properties of phenolates. In earlier studies the redox potentials of certain phenoxyl radicals harboring electron-donating substituents have been established in water.[5] For phenoxyl radicals with high redox potentials only relative estimates based on kinetics exist.[6,7]

The structural modification of the phenoxyl radicals by the substituent has also been investigated[8,9] in water solvent. In the gas phase, only the electron affinity of the unsubstituted phenoxyl radical has been measured up to date.[10]

The present work will explore the effect of para substituents on the redox properties of phenoxyl/phenolate couples in water over a large span. When combined with the acid dissociation constants of the corresponding phenols these values give a quantitative measure of the relative strengths of the phenolic O–H bond in water and at least semiquantitative ones for the corresponding bond strengths in the gas phase. Whenever gas-phase proton affinities are available the latter values allow the electron affinities of the corresponding phenoxyl radicals to be predicted. The use of thermochemical cycles to predict gas-phase properties from liquid-state measurements or vice versa was pioneered by Eberson.[11] Extensive use of this method has been made in a series of papers by Bordwell et al.[12-14] where the cycles are described in detail.

Experimental Section

The pulse radiolysis equipment consists of a microtron accelerator[15] delivering 7 MeV electrons and a computerized optical detection system.[16] For dosimetry air-saturated 10^{-2} M KSCN solutions were employed. The $G\epsilon$ value of the $(SCN)_2^{\bullet-}$ radical was taken to be 2.2×10^{-4} m^2/J at 500 nm.[17] All experiments were performed in N_2O-saturated aqueous solutions where the primary radiation chemical yield of $OH^{\bullet}$ radicals, G_{OH}, was set to 5.6×10^{-7} mol/J. The pH was sufficiently high for more than 95% of the phenols to be in the deprotonated form, i.e., in most cases between 11 and 12. The primary oxidation of the phenolates was achieved by $N_3^{\bullet}$ produced in the reaction of $OH^{\bullet}$ radicals with N_3^- which was added in sufficient excess to scavenge at least 90% of the $OH^{\bullet}$ radicals. The pulses employed were $1-2 \times 10^{-7}$ s long generating total radical concentrations on the order of 10^{-6} M.

$NaClO_2$ was purified according to ref. 18. The various phenols, 1-Me-Indole (Aldrich, purest grade available), NaN_3, KSCN, KI and the various buffers (Merck, p a quality) were employed without purifi-

(1) Arnett, E. M.; Small, L. E.; Oancea, D.; Johnston, D. *J. Am. Chem. Soc.* **1976**, *98*, 7346.
(2) Bolton, P. D.; Hepler, L. G. *Q. Rev., Chem. Soc.* **1971**, *4*, 521.
(3) McMahon, T. B.; Kebarle, P. *J. Am. Chem. Soc.* **1977**, *99*, 2222.
(4) Fujio, M.; McIver, R. T., Jr.; Taft, R. W. *J. Am. Chem. Soc.* **1981**, *103*, 4017.
(5) Steenken, S.; Neta, P. *J. Phys. Chem.* **1982**, *86*, 3661.
(6) Neta, P.; Maruthamuthu, P.; Carton, P. M.; Fessenden, R. W. *J. Phys. Chem.* **1978**, *82*, 1875.
(7) Alfassi, Z. B.; Huie, R. E.; Neta, P. *J. Phys. Chem.* **1986**, *90*, 4156.
(8) Schuler, R. H.; Neta, P.; Zemel, H.; Fessenden, R. W. *J. Am. Chem. Soc.* **1976**, *98*, 3825.
(9) Tripathi, G. N. R.; Schuler, R. H. *J. Phys. Chem.* **1988**, *92*, 5129.
(10) Richardson, J. H.; Stephenson, L. M.; Brauman, J. T. *J. Chem. Phys.* **1975**, *62*, 1580.
(11) Eberson, L. *Acta Chem. Scand.* **1963**, *17*, 2004.
(12) Bordwell, F. G.; Bausch, M. J. *J. Am. Chem. Soc.* **1986**, *108*, 2473.
(13) Bordwell, F. G.; Cheng, J.-P.; Harrelson, J. A., Jr. *J. Am. Chem. Soc.* **1988**, *110*, 1229.
(14) Bordwell, F. G.; Cheng, J.-P. *J. Am. Chem. Soc.* **1989**, *111*, 1792.
(15) Rosander, S. Thesis, Royal Institute of Technology, Stockholm 1974; TRITAEEP-74-16, p 28.
(16) Eriksen, T. E.; Lind, J.; Reitberger, T. *Chem. Scr.* **1976**, *10*, 5.
(17) Fielden, E. M. In *The Study of Fast Processes and Transient Species by Electron Pulse Radiolysis*; Baxendale, J. H., Busi, F., Eds.; Reidel: Dordrecht, Holland, 1982; Nato Advanced Study Institutes Series; pp 49-62.
(18) Eriksen, T. E.; Lind, J.; Merényi, G. *J. Chem. Soc., Faraday Trans. 1* **1981**, *77*, 2115.

0002-7863/90/1512-479$02.50/0